Science of the Total Environment 807 (2022) 151050

Contents lists available at ScienceDirect

Science of the Total Environment

journal homepage: www.elsevier.com/locate/scitotenv

Short Communication

Mine tailings in a redox-active environment: Iron geochemistry and potential environmental consequences

Hermano Melo Queiroz [a], Francisco Ruiz [a], Youjun Deng [b], Valdomiro S. de Souza Júnior [c], Amanda Duim Ferreira [a], Xosé Luis Otero [d], Danilo de Lima Camêlo [e], Angelo Fraga Bernardino [f], Tiago Osório Ferreira [a,*]

[a] Department of Soil Science, "Luiz de Queiroz" College of Agriculture, University of São Paulo, Piracicaba, São Paulo, Brazil
[b] Department of Soil and Crop Sciences, Texas A&M University, College Station, TX, USA
[c] Universidade Federal Rural de Pernambuco, Departamento de Agronomia, Av. Dom Manoel de Medeiros, s/n, 52171-900 Recife, PE, Brazil
[d] CRETUS Institute, Departamento de Edafología y Química Agrícola, Facultad de Biología, Universidad de Santiago de Compostela, Spain
[e] Department of Agronomy, Federal University of Espírito Santo, Alegre, Espírito Santo State, Brazil
[f] Department of Oceanography, Universidade Federal do Espírito Santo, Vitória, Espírito Santo 29075-910, Brazil

HIGHLIGHTS

- Within four years, the iron oxides in the tailings underwent fast geochemical changes.
- A sharp decrease in crystallinity led to high susceptibility to dissolution.
- Redox conditions in the estuarine environment favored poorly crystalline Fe oxides.
- Mean crystal size of Fe oxides decreased over time increasing its reactivity.
- The overall geochemical changes affect the fate of potentially detrimental elements.

GRAPHICAL ABSTRACT

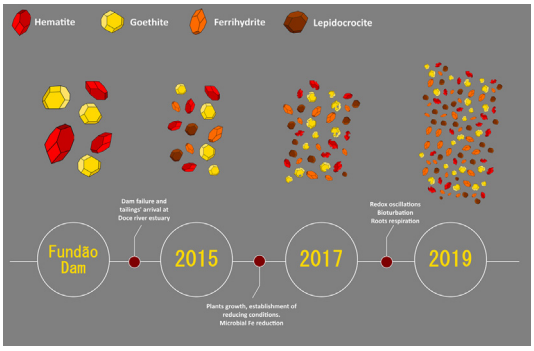

ARTICLE INFO

Article history:
Received 14 September 2021
Received in revised form 13 October 2021
Accepted 14 October 2021
Available online 19 October 2021

Editor: Filip M.G. Tack

Keywords:
Mariana's disaster
iron oxyhydroxides
Crystallinity
Fe minerals
Fe geochemistry

ABSTRACT

Iron (Fe) oxyhydroxides provide many functions in soils, mainly owing to their large surface area and high surface charge density. The reactivity of Fe oxyhydroxides is function of their mineralogical characteristics (e.g., crystallinity degree and crystal size). Detailed studies of these features are essential for predicting the stability and reactivity of these minerals within soil and sediments. The present study aimed to evaluate geochemical changes in Fe-rich tailings after the world's largest mining disaster in SE Brazil (in 2015) and to predict the potential environmental implications for the estuary. The mineralogical characteristics of the tailings were studied at three different times (2015, 2107, and 2019) to assess how an active redox environment affects Fe oxyhydroxides and to estimate the time frame within which significant changes occur. The study findings indicate a large decrease in the Fe oxyhydroxides crystallinity, which were initially composed (93%) of highly crystalline Fe oxyhydroxides (i.e., goethite and hematite) and 6.7% of poorly crystalline Fe oxyhydroxides (i.e., lepidocrocite and ferrihydrite). Within 4 years the mineralogical features of Fe oxyhydroxides had shifted, and in 2019 poorly crystalline Fe oxyhydroxides represented 47% of the Fe forms. Scanning electron microscope micrographs and the mean crystal size evidenced a decrease in particle size from 109 nm to 49 nm for goethite in the d_{111} direction. The changes in mean crystal size increased the reactivity of Fe oxyhydroxides, resulting in a greater number of interactions with cationic and anionic species. The decreased crystallinity and increased reactivity led to the compounds being more susceptible to reductive dissolution. Overall, the findings show

* Corresponding author.
E-mail address: toferreira@usp.br (T.O. Ferreira).

https://doi.org/10.1016/j.scitotenv.2021.151050

that the decrease in crystallinity along with higher susceptibility to reductive dissolution of Fe oxyhydroxides can affect the fate of environmentally detrimental elements (e.g., phosphorus and trace metals) thereby increasing the concentration of these pollutants in estuarine soils and waters.

1. Introduction

Iron (Fe) ore production is one the most important mining activities worldwide, with an annual production of approximately 3000 Mt. (Lu, 2015). However, Fe mining also generates tons of tailings, which are usually stored in dams (Glombitza and Reichel, 2014; Lu, 2015; Zheng et al., 2011). The tailings are mainly composed of fine particles that are rich in Fe oxides and hydroxides (e.g. hematite, goethite, maghemite, and magnetite) and minor amounts of quartz, kaolinite, gibbsite, and pyrite (Botha and Soares, 2015; Lu, 2015; Silva et al., 2020; Zhang et al., 2006).

Fe oxyhydroxides (here including oxides, hydroxides, and oxyhydroxides) commonly occur as nanoparticles in soils and sediments (Faivre and Frankel, 2016; Fontes and Weed, 1991). Due to their small particle size (as small as 1 or 2 nm), large specific surface area (up to 600 $m^2\ g^{-1}$) and large number of structural defects, Fe oxyhydroxides are among the most reactive minerals found in terrestrial environments (Cornell and Schwertmann, 2003; Schwertmann, 1988).

Several Fe oxyhydroxides have been recognized, and most of them are common in natural environments (Bigham et al., 2002; Faivre and Frankel, 2016). However, only eight are frequently found in soils and sediments, e.g., hematite, maghemite, magnetite, ferrihydrite, green rust, goethite, lepidocrocite, and schwertmannite (Bigham et al., 2002). The structure of Fe oxyhydroxides consists of closely packed arrays of anions (O^{2-} or OH^{-}), commonly forming three-dimensional arrangements such as octahedral and/or tetrahedral packings (Schwertmann and Taylor, 1989). The large specific surface area of these compounds (often >100 $m^2\ g^{-1}$) and the variability of minerals is a result of the arrangement of $Fe(O/OH)_6$, FeO_6, or FeO_4 (Bigham et al., 2002; Cornell and Schwertmann, 2003).

In soils, Fe oxyhydroxides play numerous important/relevant functions such as providing sorption sites for essential nutrients (e.g., phosphorus; Fink et al., 2016), promoting organo-mineral interactions that increase soil organic matter stabilization (Wang et al., 2019) and attenuating contamination by immobilizing potentially toxic elements (e.g., trace metals; Herbert, 1996; Rutten and de Lange, 2003; Sherameti and Varma, 2015). Within the upland soils, Fe oxyhydroxides are poorly soluble at a wide range of pH (4–10) and in the absence of complexing (e.g., organic compounds) or reducing environments (e.g., anaerobic media). Under these environments, Fe oxyhydroxides generally exhibit high stability (Benjamin et al., 1996; Cornell and Schwertmann, 2003; Hartley et al., 2004).

By contrast, in wetland soils and sediments, Fe oxyhydroxides present lower stability in response to redox variations (Cummings et al., 2000; Schwertmann, 1991). The reductive dissolution of Fe oxyhydroxides can take place under suboxic and/or anoxic soil conditions (Lovley, 1991; Reddy and DeLaune, 2008). This is a conspicuous process in estuarine soils and sediments where these redox conditions probably occur (Reddy and DeLaune, 2008). Reduction of Fe oxyhydroxides promotes mineral dissolution and also the release of adsorbed cations and anions (Bonneville et al., 2004; Lovley et al., 2004).

In addition to being affected by the soil geochemical environment, the dissolution of Fe oxyhydroxides can also be affected by some intrinsic properties of the minerals; e.g., surface area, degree of crystallinity, and isomorphic Al-substitution (Cornell and Schwertmann, 2003; Fontes and Weed, 1991). These characteristics are interrelated, and the combined effects on mineral dissolution are associated with structural disorders, crystal defects (e.g. vacancies), and increased number of surface interactions, resulting in a weakening of the Fe—O bonds, ultimately increasing the susceptibility of Fe oxyhydroxides to dissolution (Larsen and Postma, 2001; Ruan and Gilkes, 1995; Strauss et al., 1997).

Detailed studies of the mineralogical characteristics of Fe oxyhydroxides are essential for predicting the stability and reactivity of these minerals in soils and sediments, as well as the potential release of associated elements, such as potentially toxic elements (e.g., trace metals; Buekers et al., 2008; Cui et al., 2020; Gomes et al., 2017; Harford et al., 2015; Pereira et al., 2008).

Thus, the present study aimed to assess the mineralogical changes in Fe oxyhydroxide-rich mine tailings deposited in the Doce River estuary (SE Brazil) in 2015 after the world's largest mining disaster (Carmo et al., 2017; Escobar, 2015). We performed a detailed mineralogical assessment in different years (2015, 2017, and 2020) by using X-ray diffraction (XRD), attenuated total reflectance Fourier transform infrared (ATR-FTIR) and scanning electron microscopy (SEM) in addition to different types of chemical analysis, such as elemental analysis and sequential extraction procedures.

The Doce River estuary provides a unique framework enabling assessment of how an active redox environment, driven by tide regime, affects Fe oxyhydroxides and also estimation of the time frame within which significant mineralogical changes may occur. Previous studies in the same study area have reported the presence of potentially toxic elements and phosphorus associated with Fe oxyhydroxides in the mine tailings (Queiroz et al., 2018a; Gabriel et al., 2020). Thus, the present study is important for determining the actual role of Fe oxyhydroxides in the fate of these environmentally detrimental elements (Queiroz et al., 2018a, 2021a; Bernardino et al., 2019).

2. Materials and methods

2.1. Study site and sampling

The study site is located at the Doce River estuary, SE Brazil (19°38′–19°45′S and 39°45′–39°55′W; Fig. 1) which, after failure of the Fundão dam in 2015, received a large quantity of fine textured Fe-rich mining tailings (Gomes et al., 2017; Queiroz et al., 2018a). The estuarine region is characterized by two distinct climate seasons: a dry season, between April and September, and a wet season marked by peaks in river flooding, between October and March (de Mello et al., 2012; Gabriel et al., 2020). Moreover, in the Doce River estuary, there is a diurnal tide regime and a high input of freshwater which favors the occurrence of periodically flooded soils (Bernardino et al., 2018).

In the estuary, field sampling was conducted at three different times. The first sampling campaign was conducted in 2015, seven days after arrival of the tailings to the estuary. The other two field campaigns were performed in 2017 and 2019, i.e., two and four years after the disaster. The estuarine soil samples were collected down to 40 cm depth using polyvinyl chloride tubes attached to a waterlogged soil sampler (Howard et al., 2014; LaForce et al., 2000; Otero et al., 2009). The sampling locations were recorded to enable the same sites to be sampled in the different years. The samples were hermetically sealed and transported in a vertical position at a temperature of approximately 4 °C (Barcellos et al., 2019; Howard et al., 2014; LaForce et al., 2000; Nóbrega et al., 2014). In the laboratory, the most representative soil layer of deposited tailings (i.e., up to 0–15 cm layer) was selected and immediately analyzed. Additionally, a sample of tailing collected inside the Fundão dam was provided by the Brazilian National Mining Agency.

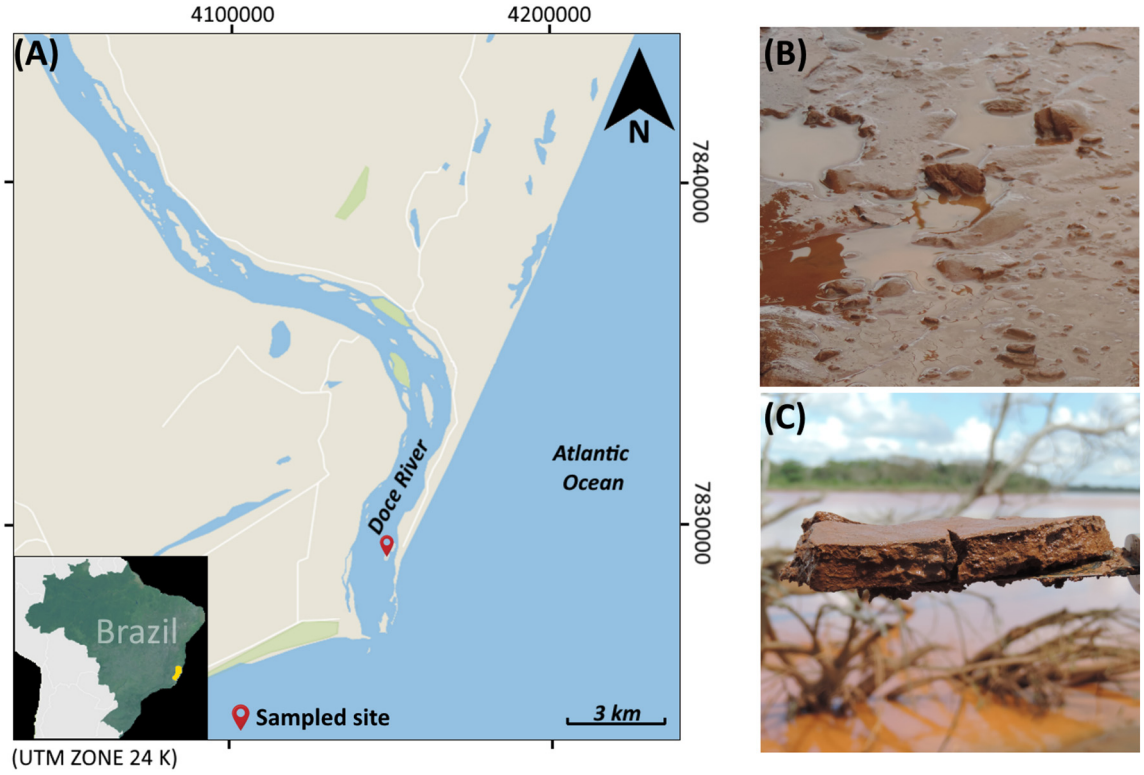

Fig. 1. (A) Location of the study site in the Doce River estuary, in the municipality of Regência, Espírito Santo state, Brazil. In detail, (B) the freshly deposited Fe tailings on the estuarine soils in 2015 and (C) the sampled ~5 cm layer of the Fe-rich fine textured tailing deposited in the estuary.

The pH and redox potential (Eh) values of all samples were measured in the field with portable meters (HANNA, model HI98121). The pH was measured with a glass electrode, previously calibrated with standard solutions (pH 4.0 and 7.0). The Eh values were recorded with a platinum electrode tested with a quality control solution (HI7021M 240 mV, 25 °C ORP Test Solution), and the values were adjusted by adding the value for the calomel reference electrode (+244 mV S.H.E.).

2.2. X-ray diffraction and calculation of mean crystal size (MCS)

The mineralogy of the clay fraction (<2 μm) was determined with an X-ray diffractometer (Rigaku Miniflex II), with CuKα radiation. The selected samples and tailing were scanned from 20 to 60° 2θ, step size of 0.02° 2θ and counting time of 5 s step^{-1}. Before analysis, the samples were treated with 9% sodium hypochlorite to remove organic matter, and sand was removed by wet sieving after dispersion of the suspension with 0.01 mg L^{-1} Na_2CO_3 (Siregar et al., 2005). Subsequently, the dried clay fraction (grounded at 0.25 mm) was obtained after separation from the silt fraction by the sedimentation method (Stoke's law; Jackson, 2005) and analyzed (powder sample; Pansu and Gautheyrou, 2006).

The mean crystal size (MCS) was calculated from the width of the half-height of the reflexes for goethite (d_{110} and d_{111} planes) and hematite (d_{012} and d_{110} planes) using the Scherrer formula (see Klug and Alexander, 1974) and after correcting the width at half-height using NaCl as an internal standard (Singh and Gilkes, 1992).

2.3. Attenuated total reflectance Fourier transform infrared (ATR-FTIR) analysis

ATR–FTIR data were obtained with a spectrometer (PerkinElmer Spectrum Two), with N_2 as the purge gas. Spectra were acquired via a diamond crystal (45° angle of incidence). The tailings and selected samples were macerated in an agate mill prior to data collection. The samples were arranged over the entire crystal and were then pressed at a constant force of 115 N. The spectra were obtained at a spectral range of 400 cm^{-1} to 4000 cm^{-1}. A total of 50 co-added spectra were obtained for each spectrum, at a resolution of 4 cm^{-1}, and adjusted using the attenuated total reflectance (ATR) method.

2.4. Scanning electron microscopy (SEM) analysis

SEM photomicrographs of the samples were obtained using a SU8010 cold field emission scanning electron microscope (FESEM, Hitachi, Japan). Elemental analysis was carried out using an energy-dispersive X-ray spectroscopy (EDS, AMETEK-EDAX, USA) attached to the scanning electron microscope. For EDS analysis, the selected samples and tailings were anchored tightly to the surface of the conducting tape after coating with a thin layer (0.5–15 nm) of gold, and they were then transferred directly to the microscope.

2.5. Fe sequential chemical extraction

Sequential extraction of Fe was carried out using a combination of methods proposed by Tessier et al. (1979), Huerta-Diaz and Morse (1990), and Fortin et al. (1993). The combined method enables the determination of six distinct fractions (Table 1), operationally defined as follows: exchangeable and soluble Fe (FeEX); Fe bound to carbonates (FeCA); Fe bound to ferrihydrite (FeFR), lepidocrocite (FeLP), crystalline Fe oxyhydroxides (i.e., goethite and hematite, FeCR); and pyritic Fe (FePY). For additional details, see Ferreira et al. (2007a), Otero et al. (2009), and Machado et al. (2014).

The Fe concentrations were obtained by an Inductively Coupled Plasma - optical emission spectrometer (Thermo Fisher Scientific, Waltham). Curve calibration solutions were prepared by dilution of certified Fe standard solution (43149-100ML-F) and certified reference material

Table 1
Description of solid-phase fractionation analysis of iron (Fe) according to Tessier et al. (1979), Huerta-Diaz and Morse (1990), and Fortin et al. (1993).

Fraction	Abbreviation	Chemical Extractor[a]/Procedure
Exchangeable and soluble Fe	FeEX	Extracted with a 1 mol L^{-1} $MgCl_2$ solution at pH adjusted to 7. Agitation for 30 min and then centrifuged at 10,000 rpm for 30 min.
Fe bound to carbonates	FeCA	Extracted with a 1 mol L^{-1} NaOAc (sodium acetate) solution at pH 5. Agitation for 5 h and then centrifuged at 10,000 rpm for 30 min.
Fe bound to ferrihydrite	FeFR	Extracted with a 0.04 mol L^{-1} hydroxylamine + acetic acid 25% (v/v) solution. Agitation for 6 h at 30 °C and then centrifuged at 10,000 rpm for 30 min.
Fe bound to lepidocrocite	FeLP	Extracted with a 0.04 mol L^{-1} hydroxylamine + acetic acid 25% (v/v) solution. Agitation for 6 h at 96 °C and then centrifuged at 10,000 rpm for 30 min.
Fe bound to hematite and goethite, i.e., high crystallinity Fe phases	FeCR	Extracted with a 0.25 mol L^{-1} sodium citrate +0.11 mol L^{-1} sodium bicarbonate solution and 3 g of sodium dithionite. Agitation for 6 h at 75 °C and then centrifuged at 10,000 rpm for 30 min.
Pyritic Fe	FePY	Extracted with concentrated HNO_3. The samples were agitated for 2 h then washed with 15 mL of ultrapure water. Before extraction the samples were subjected to treatment with 10 mol L^{-1} HF to remove phyllosilicates, and concentrated H_2SO_4 was then added to remove Fe associated with organic matter

[a] All used solutions and centrifuge tubes were purged with N_2 flow to guarantee a free oxygen condition. Between each extraction the residue from prior step was washed twice with 20 mL of deoxygenated Milli-Q water.

(SRM 2709a San Joaquin) was used to guarantee the quality control procedures. The Fe concentration recovery values were above 90%.

3. Results

3.1. Physicochemical conditions

The Eh (+360 mV) and pH (6.0) values of the tailings sample from inside the Fundão dam were characteristic of oxidizing conditions (> +300 mV; Reddy and DeLaune, 2008) (Fig. 2). In the estuary, immediately after the disaster (in 2015), the Eh and pH values were respectively +64 mV and 7.0, indicating moderately reducing conditions (0 to +300 mV; Fig. 2). In 2017, the Eh (−114 mV) and pH (7.0) values indicated reduced conditions (Eh values <0 mV; Fig. 2). In 2019 (four years after the arrival of the tailings), the conditions were moderately reducing (Eh = 44 mV; pH = 6.0; Fig. 2).

3.2. X-ray diffraction and mean crystal size (MCS)

The clay XRD patterns of the tailings sample showed the presence of goethite (0.157, 0.173, 0.181, 0.193, 0.219, 0.226, 0.245, 0.258, 0.269, 0.338 and 0.418 nm; Fig. 3), hematite (0.160, 0.169, 0.184, 0.269, 0.252, and 0.371 nm) and kaolinite (0.234, 0.358 nm). In the estuary samples obtained in 2015, 2017, and 2019, the clay XRD patterns showed a similar mineralogical assemblage, also with the presence of goethite (0.157, 0.258, 0.245, 0.338, and 0.418 nm; Fig. 3), hematite (0.157, 0.169, 0.184, 0.252, and 0.269 nm), and kaolinite (0.234, 0.358 nm) (Fig. 3).

In addition, sharper goethite peaks (at 0.418, 0.269, 0.245, 0.219, 0.193, 0.181, and 0.172 nm) were observed in the tailings sample, and the sharpness gradually decreased in the estuary samples collected in 2015, 2017, and 2019. For hematite, sharper peaks were also observed in the tailings sample (0.371, 0.269, 0.252, and 0.184 nm; Fig. 3), but decreased gradually in the estuary samples collected in 2015, 2017, and 2019.

The mean crystal size (MCS) of goethite in the d_{110} direction was 56.14 nm for the tailings sample and 86.25, 42.93, and 29.78 nm for the estuary samples from 2015, 2017, and 2019 respectively (Table 2). The MCS of goethite in the d_{111} direction was 109.38 nm for the tailings and 87.50, 61.70, and 48.62 nm for the estuary samples collected in 2015, 2017, and 2019 (Table 2). In the tailings sample, the MCS of hematite was 54.89 and 82.76 nm for the d_{012} and d_{110} directions, respectively. For the estuary samples from 2015, 2017, and 2019, the MCS values of hematite were not calculated for the d_{012} and d_{110} planes due to absence or overlapping of peaks, and irregular peak morphology (Fig. 3).

3.3. ATR-FTIR results

The tailings showed bands at 3131 to 532 cm^{-1}, assigned to Fe oxyhydroxides, and at 3131, 1650, 1008, and 798 cm^{-1} due to the stretching vibration of O—H bonds assigned to goethite. The lower stretching band at 532 cm^{-1} was assigned to hematite (Fig. 4; Chukanov, 2014).

In the samples collected in the Doce River estuary in 2015, 2017, and 2019, bands assigned to Fe oxyhydroxides were observed at 2985 to 452 cm^{-1} (Fig. 4). The most prominent bands in the estuary samples occurred at 1003, 793, and 749 cm^{-1} (Fig. 4), i.e. the bands typically observed for goethite and lepidocrocite (Chukanov, 2014). In addition, in all the samples from the estuary (i.e., 2015, 2017, and 2019), distinct bands assigned to ferrihydrite were observed at 1026 to 676 cm^{-1} (Fig. 4).

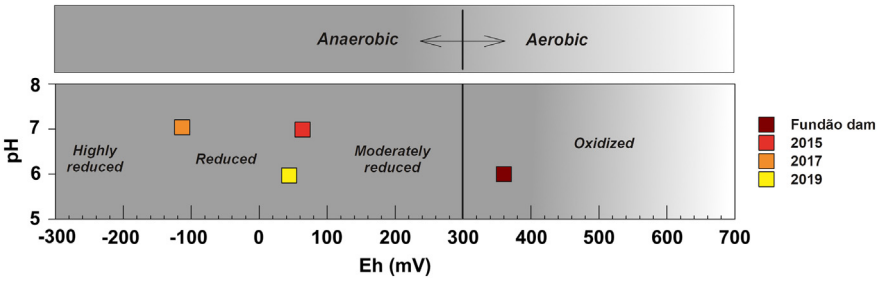

Fig. 2. Eh-pH diagram with the data of the tailings sample from Fundão dam and the samples collected in the Doce River estuary in 2015, 2017, and 2019. The Eh-pH diagram and redox conditions (i.e., highly reduced, reduced, moderately reduced and oxidized) are adapted from Reddy and DeLaune (2008).

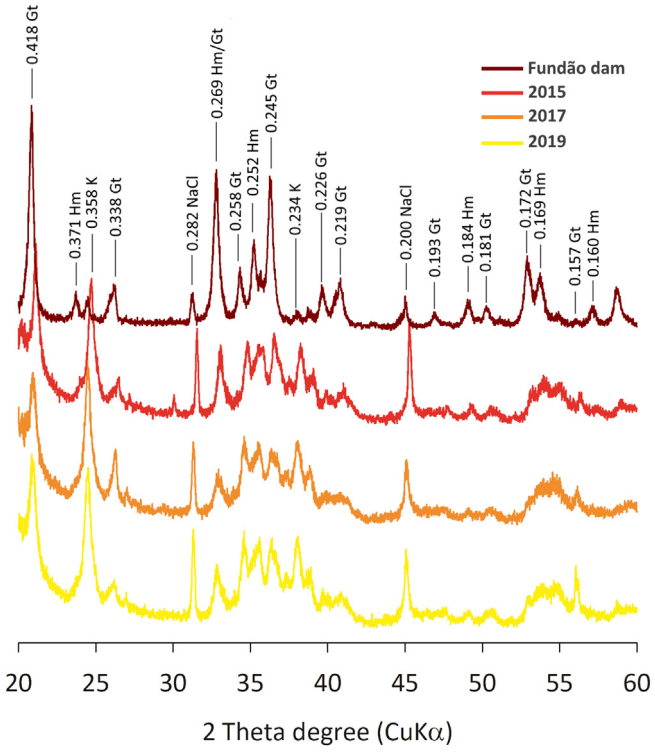

Fig. 3. XRD patterns from the tailings sample and soil samples collected in the estuary in 2015, 2017 and 2019. Kaolinite (K), Goethite (Gt), Hematite (Hm).

3.4. SEM-EDS results from tailings and estuary samples from Doce River estuary

The SEM micrographs of the tailings samples (Fig. 5A) revealed the presence of irregular (undefined shape) particles of Fe oxyhydroxides that occur naturally in soil and sediments (see Bigham et al., 2002). The presence of Fe oxyhydroxides was revealed by SEM-EDS analysis of the central part of the particles with a dominant FeO chemical composition (Fig. 5E). The SEM micrographs showed irregularly shaped particles in samples from 2015 (Fig. 5B), 2017 (Fig. 5C), and 2019 (Fig. 5D), with similar chemical composition (i.e., predominantly FeO; Fig. 5E) and also the presence of Fe oxyhydroxides. However, for these sample, the SEM micrographs revealed gradually smaller particle sizes (Fig. 5 B, C and D) relative to the mineral particles observed in the tailings sample (Fig. 5A).

3.5. Sequential extraction of Fe

The Fe sequential extraction showed that the Fe in the tailings was mainly associated with crystalline Fe oxides (FeCR: 92% Fig. 6) followed by poorly crystalline Fe oxyhydroxides (FeLP: 4% and FeFR: 0.1%; Fig. 6) and pyritic iron (FePY 4%). Fe associated with FeEX and FeCA accounted for less than 1% of total Fe.

Table 2
Corrected d-spacing and mean crystal size (MCS) of goethite (Gt) and hematite (Hm) for the clay fraction of the tailings (inside the Fundão dam) and the samples collected in the Doce River estuary in 2015, 2017, and 2019.

Sample	d-spacing (nm)[a]				MCS (nm)			
	Gt_{110}	Gt_{111}	Hm_{012}	Hm_{110}	Gt_{110}	Gt_{111}	Hm_{012}	Hm_{110}
Fundão dam	0.417	0.245	0.371	0.252	56.14	109.38	54.89	82.76
2015	0.416	0.245	n.d	0.252	86.25	87.50	n.d	n.d
2017	0.416	0.245	n.d	0.251	42.93	61.70	n.d	n.d
2019	0.417	0.244	n.d	0.251	29.78	48.62	n.d	n.d

[a] Corrected d-spacing using halite as an internal standard. N.d. = not determined.

Samples from the estuary changed significantly over time. Similarly, to the tailings, in 2015, most of the Fe was associated with crystalline oxides (FeCR: 93%), followed by the FeFR (3%) and FeLP (3% Fig. 6). The FeEX, FeCA, and FePY together also represented less than 1% of the total Fe content (Fig. 6).

However, in the following years, the data showed a marked change in the crystallinity of Fe oxyhydroxides in the estuary. In 2017 and 2019, FeCR represented 63% and 52% respectively, of the total Fe contents. By contrast, Fe associated with poorly crystalline oxyhydroxides (i.e., FeFR + FeLP) increased to 37% of total Fe in 2017 and to 47% in 2019 (Fig. 6). Fe associated with the other fractions (i.e., FeEX, FeCA, and FePY) occurred in low proportions, representing less than 1% of the total Fe (0.2 ± 0.2%), in both 2017 and 2019.

4. Discussion

4.1. The physicochemical changes

The physicochemical conditions of the tailings inside the Fundão dam indicated the existence of oxidizing conditions. However, in 2015 the soil physicochemical conditions changed to a moderately reduced environment, commonly observed in soils and sediments in estuarine environments (Cuadros et al., 2017; Nóbrega et al., 2015; Queiroz et al., 2018b). By 2017, the physicochemical conditions had become further reduced and favorable to microbial Fe reduction (Eh < 0 mV; Reddy and DeLaune, 2008). Thus, our findings clearly showed redox-active conditions in the Doce River estuary.

The more reduced physicochemical environment in the Doce River estuary is associated with organic matter inputs due to the colonization and growth of estuarine plants (i.e. *Eleocharis acutangula* and *Typha domingensis*) over the deposited tailings after the disaster (Queiroz et al., 2021b). These authors reported that after plants colonized the tailings there was significant input of organic matter (via litterfall, roots exudates, and dead roots) which favored the establishment of reducing conditions. In addition to plant growth, the daily tidal flooding and

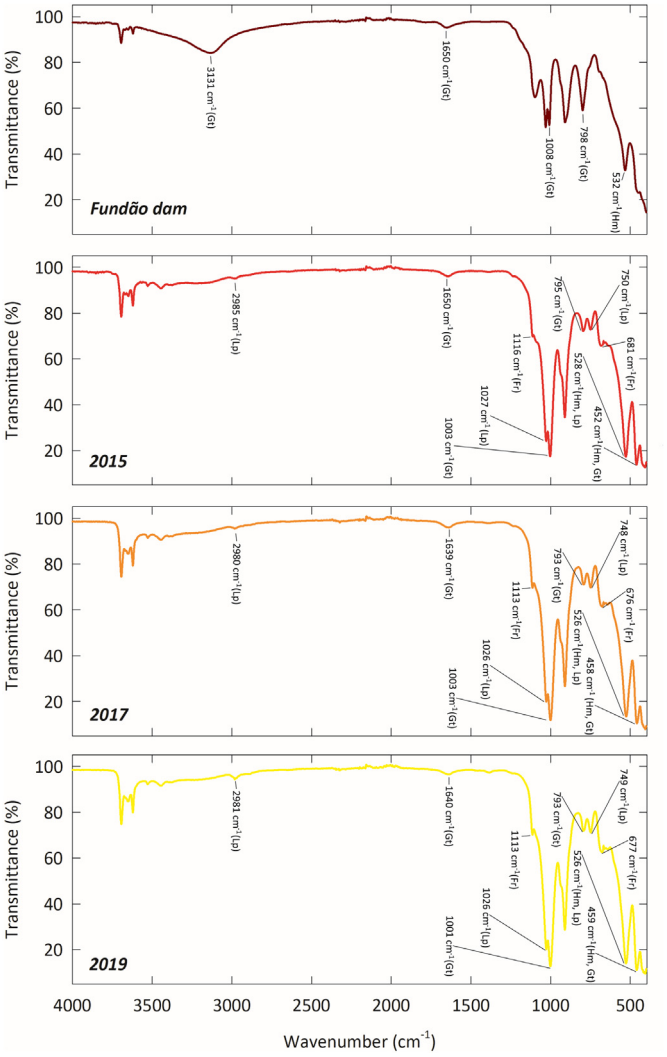

Fig. 4. Attenuated total reflection – Fourier-transform infrared spectroscopy (ATR-FTIR) spectra of the tailings sample and samples collected in the Doce River estuary in 2015, 2017 and 2019.

low O_2 diffusion, would have driven the decrease in Eh values (Queiroz et al., 2021a) and the anaerobic respiration pathways (e.g., microbial Fe reduction).

The higher Eh values recorded in 2019 may also be attributed to the effects of plant growth and root respiration (Rehman et al., 2017). Moreover, vegetation growth stimulates the presence and activity of fauna (e.g., bioturbation by crabs) in estuarine soils, further enhancing diffusion of oxygen into the estuarine soils (Fondo and Martens, 1998; Sarker et al., 2020). Crab burrows and bioturbation promote soil aeration and increase the Eh values and, thus, the oxidation of Fe (Fe^{2+}), which re-precipitates as poorly crystalline Fe oxyhydroxides (Alongi, 2010; Ferreira et al., 2007b; Nielsen et al., 2003).

4.2. Changes in mineralogy over time

The mineralogical assemblage of the tailings from inside the dam was predominantly composed of Fe oxyhydroxides and was clearly associated with the mined Fe-rich ore. The mine is located in the "*Quadrilátero Ferrífero*" a geological formation of Palaeoproterozoic banded iron formation (Itabirite) mainly composed of the Fe oxyhydroxides identified (e.g., hematite and goethite; Cabral et al., 2002; Silva et al., 2016; Gama et al., 2019). The XRD spectra showed greater intensities and sharper peaks for the hematite and goethite in the tailings, indicating higher crystallinity when compared to the surface samples from the Doce River estuary (Schulze, 1981; Schwertmann et al., 1982).

The higher MCS values (Table 2) for goethite (d_{110} plane: 56.14 nm, d_{111} plane: 109.38 nm) in the tailings sample than in the estuary samples (i.e., 2015, 2017, and 2019) corroborate a higher planes growth and crystallinity in the tailings (Camêlo et al., 2017; Singh and Gilkes, 1992). According to Fontes and Weed (1991), highly crystalline goethite with greater crystal development exhibits higher MCS values for the d_{111} plane than the d_{110} plane, indicating preferential growth in the z direction. Similarly, for hematite, the higher MCS for the d_{110} plane also indicates greater crystal development (Melo et al., 2001).

On the other hand, the samples from the different years (2015, 2017, and 2019; Fig. 3) showed XRD spectra indicative of a mineral assemblage mainly composed of lower crystalline Fe oxides with structural disorders leading to less intense, broad peaks (Camêlo et al., 2018; Cornell and Schwertmann, 2003). Thus, the lower intensity and broader peaks of hematite (0.371, 0.269, 0.252, 0.184, and 0.157 nm) and goethite (0.172, 0.193, 0.219, 0.245, 0.269, and 0.418 nm) in the samples from 2015, 2017, and 2019 (Fig. 3) are probably associated with a lower degree of crystallinity and/or loss of mineral phases (see Velde and Peck, 2002; Wang et al., 2015).

Previous studies reported that a decrease in the degree of crystallinity and/or loss of mineral phases results in lower values of MCS, more structural defects and less intense, broader XRD peaks (Camêlo et al., 2018; Fontes and Weed, 1991; Melo et al., 2001; Wang et al., 2015). Moreover, the decrease in crystallinity may reflect a higher susceptibility of Fe oxyhydroxides to undergoing reductive dissolution due to an increase both in surface area and structural disorder (see Larsen and Postma, 2001; Cornell and Schwertmann, 2003).

The lower MCS values in samples from 2015, 2017, and 2019 are supported by SEM micrographs (Fig. 5), which clearly showed smaller particle sizes in these samples (< 20 nm). In addition, the SEM micrographs of samples collected in 2015, 2017, and 2019 did not show the typical morphology of goethite (acicular; Bigham et al., 2002) or hematite (hexagonal and rhombohedral; Schwertmann et al., 2000), but rather irregular particle morphologies, also indicating particle size narrowing and ordination decay (see Schwertmann and Fitzpatrick, 1992; Gao and Schulze, 2010; Das and Hendry, 2014).

The structural disorder in the estuary samples was further corroborated by the ATR-FTIR results (Fig. 4). The more intense, sharper goethite bands at 795 cm^{-1} and 1001 cm^{-1} are associated with higher bending vibrations of OH, which may be a result of a structural disorder promoted by Al-substitution or by partial mineral dissolution leading to Fe displacement and more bonding of OH groups (Cornell and Schwertmann, 2003; Faivre and Frankel, 2016; Ruan et al., 2002). In addition, the broadening and stretching of bands at 748 cm^{-1}, at 681 to 676 cm^{-1}, and at 1026 cm^{-1} (in 2015, 2017, and 2019; Fig. 4) also result from OH stretching vibration, typical of poorly crystalline Fe oxyhydroxides (Bazilevskaya et al., 2011, 2012). On the other hand, smaller and slightly stretched bands of goethite and hematite at 3131 to 798 cm^{-1} and at 532 cm^{-1} in tailings samples (Fig. 4), were observed. These band features are associated with fewer OH surface groups and higher crystallinities. According to Ruan et al. (2002) a systematic decrease in the width of hematite and goethite bands results from hydroxyl release and the changes in Fe-OH to FeO bonding after thermal dihydroxylation, which leads to crystallization and crystal growth.

In wetland soils, hydroxylation of Fe oxyhydroxides occurs due to natural processes, mainly mediated by microorganisms and oscillations in redox conditions (Jolivet et al., 2004; Kosolapov et al., 2004; Randall et al., 1999). The Fe fractionation showed a significant and rapid shift in the distribution of Fe oxides within few years in the Doce River estuary. Thus, the data showed a marked increase in the poorly crystalline Fe oxyhydroxides (i.e., FeFR+FeLP) between 2015 (6.8%), 2017 (36.3%)

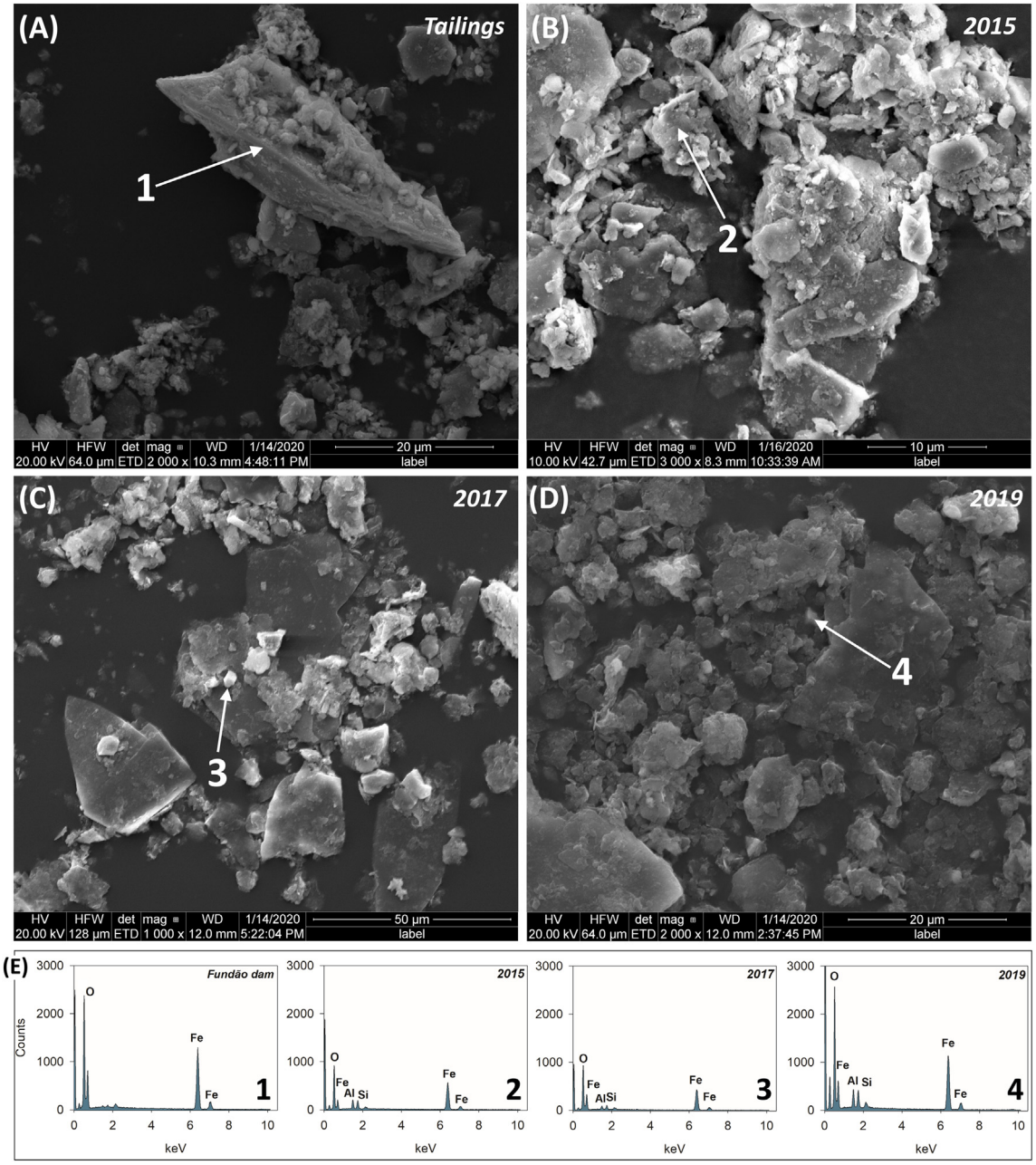

Fig. 5. Scanning electron microscopy (SEM) micrographs of the mine tailings from the Fundão dam and soil samples collected in the Doce River estuary. (A) Images from tailings samples showing irregular particles of Fe oxyhydroxides. Images of soils from (B) 2015, (C) 2017, and (D) 2019 showing an irregular shape of Fe oxyhydroxides. (E) Chemical composition determined by energy-dispersive X-ray spectroscopy (EDS) analysis of the samples and tailing.

and 2019 (47%; Fig. 6). The clear loss of crystallinity is related to the active redox conditions in the estuarine soil, which oscillated between reduced to moderately reduced conditions (see Fig. 2). Oscillations in redox conditions occur due to tidal flooding (Seybold et al., 2002), plant activity (Rehman et al., 2017), organic matter inputs to soil (Reddy and DeLaune, 2008), O_2 depletion (Du Laing et al., 2009) and fauna activity (i.e., bioturbation; Otero et al., 2020). This active redox environment favored the microbial reduction of Fe (Lovley, 1991) and the subsequent oxidation of Fe^{2+} to Fe^{3+} and, thus, its re-precipitation as poorly crystallinity Fe oxyhydroxides (Johnston et al., 2011; Lindsay, 1991; Zachara et al., 2001).

The microbial reduction of Fe consumes both the highly and poorly crystalline Fe oxyhydroxides (Kukkadapu et al., 2001; Pan et al., 2016). The Fe may be rapidly reprecipitated in the system on exposure to O_2 due to lowering tides, fauna activity or root respiration (Chen et al., 2018). Re-oxidation usually leads to precipitation of poorly crystalline Fe oxyhydroxides due to low interfacial energies of nucleation of these Fe minerals (Barcellos et al., 2018; Chen et al., 2018; Stumm and Morgan, 1996). Our results are consistent with those reported by Winkler et al. (2018) and Thompson et al. (2011), which showed that the crystallinity of Fe oxyhydroxides decreased over time after redox cycles. However, these authors reported the mineralogical changes in a paddy soil and frequently waterlogged forest soils respectively, after several decades of exposure to redox fluctuations.

The stability of reprecipitated, poorly crystalline Fe oxyhydroxides may be enhanced in the presence of Al during the crystallization process (isomorphic Al-substitution; Schwertmann, 1991; Violante et al., 2003). Indeed, Al-substitution in poorly crystalline Fe oxyhydroxides increases

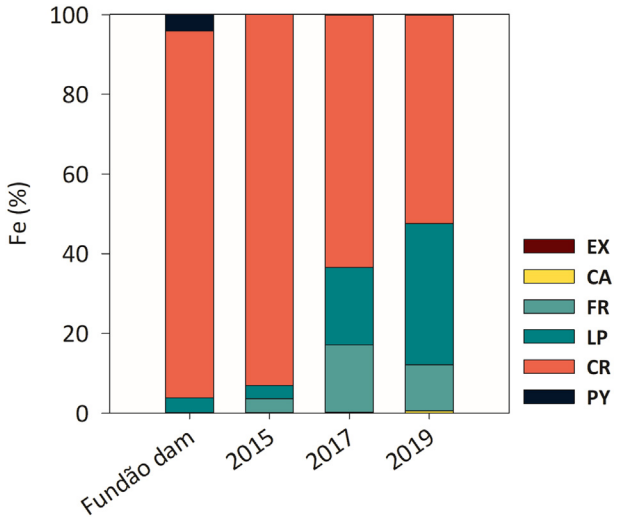

Fig. 6. Percentage of each solid phase fraction obtained by the sequential extraction procedure in the mine tailings and in samples from the Doce River estuary, collected in 2015, 2017 and 2019. EX: exchangeable Fe, CA: Fe bound to carbonates, FR: Fe bound to ferrihydrite, LP: Fe bound to lepidocrocite, CR: Fe associated with highly crystalline oxyhydroxides (i.e., hematite and goethite), and PY: pyritic Fe.

the mineral stability thus hampering reductive dissolution (Masue-Slowey et al., 2011) which is an important implication for trace metals bioavailability in redox-active environments, such as estuarine soils and sediments (Gao et al., 2021; Palau et al., 2021). The higher stability is associated with changes in structural ordering with the fortification of hydrogen bonds (Cornell and Schwertmann, 2003). Thus, despite the active-redox environment, Al-substitution may contribute to the maintenance of poorly crystalline Fe oxyhydroxides in the soil over time.

4.3. Potential environmental implications

The clear shifts in the mineralogical characteristics of Fe oxyhydroxides may have several important environmental implications for the estuarine environment in the future. Iron oxyhydroxides are known to play a role in metal retention (Hochella et al., 2005) due to their small particle size, large surface area and corresponding high reactivity (Buerge-Weirich et al., 2002; Herbert, 1996). Under oxic conditions, Fe oxyhydroxides may retain heavy metals due to the formation of inner or surface complexes such as monodentate surface hydroxo-complexes or bi-nuclear internal complexes (Cornell and Schwertmann, 2003; Grossl et al., 1994). These complexes are very stable and virtually irreversible, and they guarantee the low bioavailability of trace metals (Rose and Bianchi-Mosquera, 1993; Trivedi and Axe, 2001). However under transitory/cyclic anoxic conditions, Fe oxyhydroxides undergo reductive dissolution, which leads to a decrease in their stability and in their capacity to retain metals (Herbert, 1996; Queiroz et al., 2021b).

Due to their smaller size (2–6 nm) and higher surface area (200 to 600 $m^2\ g^{-1}$), the poorly crystalline Fe oxyhydroxides (Manceau et al., 2000; Randall et al., 1999; Roden and Zachara, 1996) have a greater potential to adsorb and immobilize both cationic and anionic species. Indeed, several studies have reported the high capacity of poorly crystalline Fe oxyhydroxides (e.g., ferrihydrite and lepidocrocite) to promote the immobilization of heavy metals in different soils (Baleeiro et al., 2018; Cornell and Schwertmann, 2003; Komárek et al., 2013; Manceau et al., 2000; Martínez, 1998; Tack et al., 2006). Similarly, P retention in poorly crystallinity Fe oxyhydroxides is also a widely reported and well-known phenomenon (Arai and Sparks, 2001; Liao et al., 2020; Slomp et al., 1996; Wang et al., 2013), which plays an important role in the eutrophication process (Kraal et al., 2015; Queiroz et al., 2021a; Wilson et al., 2004).

The poorly crystalline Fe oxyhydroxides are characterized by short-range-order, surface imperfections and weak Fe-OH bonds, which favor edge dissolution (Cornell and Schwertmann, 2003). With further dissolution, the crystals gradually become smaller and have a higher surface area (Larsen and Postma, 2001). These characteristics account for the intense dissolution rate (Bonneville et al., 2004). In response to these characteristics, the associated metals, including Fe, and phosphorus will become bioavailable (Schwertmann, 1991; Larsen and Postma, 2001; Queiroz et al., 2021b), thus posing a severe environmental risks to the Doce River estuary. In fact, previous studies reported high concentrations of metals (Queiroz et al., 2018a, 2021a) and phosphorus (Queiroz et al., 2021b) associated with the estuarine Fe oxyhydroxides. Thus, the mineralogical changes caused by the active redox environment, such as the smaller particle size observed in SEM micrographs (Fig. 5), lower MCS (Table 2), and decreased crystallinity (Figs. 4, 6), confirm the higher susceptibility to mineral dissolution in the Doce River estuarine soil. The mineral changes may lead to an increase in the concentration of pollutants (e.g., metals and phosphorus) in the soil and water from the Doce River estuary in the near future. Indeed, Queiroz et al. (2021a, 2021b) recently reported an increase in phosphorus and metal bioavailability associated with soil Fe loss due to reductive dissolution.

5. Conclusions

The tailings from inside the Fundão dam were initially mainly composed of highly crystalline Fe oxyhydroxides (e.g., goethite and hematite). In 2015, after failure of the dam, the tailings were exposed to an oscillating redox environment in the Doce River estuary. The new biogeochemical conditions decreased the crystallinity of Fe oxyhydroxides between 2015 and 2019. Our findings reveal a rapid change (within four years) in the mineralogical assemblage. The mineralogical shifts were driven by the microbial-mediated reductive dissolution, plant growth, root respiration and fauna activity. Within this period, the data showed a change from a dominance (92%) of highly crystalline Fe oxyhydroxides (goethite and hematite) to a greater presence (47%) of poorly crystallinity Fe oxyhydroxides (e.g., lepidocrocite and ferrihydrite) with smaller particle size (from 109 nm to 49 nm for goethite, d_{111} direction) and higher reactivity.

The decreased crystallinity of Fe oxyhydroxides led to the minerals becoming more susceptible to dissolution. These changes decreased the capacity of the minerals to retain both cationic and anionic elements (e.g., metals and phosphorus), thereby potentially increasing the concentration of these pollutants in estuarine soils and waters.

CRediT authorship contribution statement

Hermano M. Queiroz: First author, Writing - Reviewing and Editing, conceptualization of ideas and formulation, field work, and acquisition of the financial support.

Francisco Ruiz: Conceptualization, writing - reviewing and editing, data Curation, formal analysis, field work, and Validation.

Youjun Deng: Writing - reviewing and editing, conceptualization of ideas, validation, formal analysis, field work and data curation.

Valdomiro S. de Souza Júnior: Writing - reviewing and editing, conceptualization of ideas, Data curation, Formal analysis, Field work, and Resources.

Amanda Duim Ferreira: Writing - reviewing and editing, data curation, formal analysis, funding acquisition, and validation.

Xosé L. Otero: Writing - reviewing and editing, data curation, and formal analysis.

Danilo de Lima Camêlo: Writing - reviewing and editing, data curation.

Tiago Osório Ferreira: Acquisition of the financial support, conceptualization of ideas, field work. Provision of study materials, reagents,

materials, and instrumentation. Writing and critical reviews. Project administration.

Declaration of competing interest

The authors declare that they have no known competing financial interests or personal relationships that could have appeared to influence the work reported in this paper.

Acknowledgements

This work received financial support from the Fundação de Amparo à Pesquisa e Inovação do Espírito Santo (FAPES, grant number 77683544), Coordenação de Aperfeiçoamento de Pessoal de Nível Superior CAPES (Finance Code 001), Conselho Nacional de Desenvolvimento Científico e Tecnológico (CNPq, grant numbers 301161/2017-8 and 305996/2018-5 to AFB and TOF, respectively), São Paulo Research Foundation (FAPESP, grant numbers 2018/04259-2, 2018/08408-2, 2019/18324-3, 2019/17413-2, 2019/14800-5, and 2019/19987-6), and Xunta de Galicia-Consellería de Educación e Ordeanción Universitaria de Galicia (Consolidation of competitive groups of investigation; GRC GI 1245).

References

Alongi, D.M., 2010. Dissolved iron supply limits early growth of estuarine mangroves. Ecology 91, 3229–3241. https://doi.org/10.1890/09-2142.1.

Arai, Y., Sparks, D.L., 2001. ATR–FTIR spectroscopic investigation on phosphate adsorption mechanisms at the ferrihydrite-water Interface. J. Colloid Interface Sci. 241, 317–326. https://doi.org/10.1006/jcis.2001.7773.

Baleeiro, A., Fiol, S., Otero-Fariña, A., Antelo, J., 2018. Surface chemistry of iron oxides formed by neutralization of acidic mine waters: removal of trace metals. Appl. Geochem. 89, 129–137. https://doi.org/10.1016/j.apgeochem.2017.12.003.

Barcellos, D., Cyle, K.T., Thompson, A., 2018. Faster redox fluctuations can lead to higher iron reduction rates in humid forest soils. Biogeochemistry 137, 367–378. https://doi.org/10.1007/s10533-018-0427-0.

Barcellos, D., Queiroz, H.M., Nóbrega, G.N., de Oliveira Filho, R.L., Santaella, S.T., Otero, X.L., Ferreira, T.O., 2019. Phosphorus enriched effluents increase eutrophication risks for mangrove systems in northeastern Brazil. Mar. Pollut. Bull. 142, 58–63. https://doi.org/10.1016/j.marpolbul.2019.03.031.

Bazilevskaya, E., Archibald, D.D., Aryanpour, M., Kubicki, J.D., Martínez, C.E., 2011. Aluminum coprecipitates with fe (hydr)oxides: does isomorphous substitution of Al3+ for Fe3+ in goethite occur? Geochim. Cosmochim. Acta 75, 4667–4683. https://doi.org/10.1016/j.gca.2011.05.041.

Bazilevskaya, E., Archibald, D.D., Martínez, C.E., 2012. Rate constants and mechanisms for the crystallization of Al nano-goethite under environmentally relevant conditions. Geochim. Cosmochim. Acta 88, 167–182. https://doi.org/10.1016/j.gca.2012.04.026.

Benjamin, M.M., Sletten, R.S., Bailey, R.P., Bennett, T., 1996. Sorption and filtration of metals using iron-oxide-coated sand. Water Res. 30, 2609–2620. https://doi.org/10.1016/S0043-1354(96)00161-3.

Bernardino, A.F., Reis, A., Pereira Filho, A.C.D., de Oliveira Gomes, L.E., Bissoli, L.B., de Barros, F.C.R., 2018. Benthic estuarine assemblages of the Eastern Marine Brazilian Ecoregion (EME). In: Lana, P. da C., Bernardino, A.F. (Eds.), Brazilian Marine Biodiversity. Springer International Publishing, Cham, pp. 95–116 https://doi.org/10.1007/978-3-319-77779-5_4.

Bernardino, A.F., Pais, F.S., Oliveira, L.S., Gabriel, F.A., Ferreira, T.O., Queiroz, H.M., Mazzuco, A.C.A., 2019. Chronic trace metals effects of mine tailings on estuarine assemblages revealed by environmental DNA. PeerJ 7, e8042. https://doi.org/10.7717/peerj.8042.

Bigham, J.M., Fitzpatrick, R.W., Schulze, D.G., 2002. Iron oxides. Soil Mineralogy with Environmental Applications. Soil Science Society of America, Madison, Wisconsin, pp. 323–366 https://doi.org/10.2136/sssabookser7.c10.

Bonneville, S., Van Cappellen, P., Behrends, T., 2004. Microbial reduction of iron(III) oxyhydroxides: effects of mineral solubility and availability. Chem. Geol. 212, 255–268. https://doi.org/10.1016/j.chemgeo.2004.08.015.

Botha, L., Soares, J.B.P., 2015. The influence of tailings composition on flocculation. Can. J. Chem. Eng. 93, 1514–1523. https://doi.org/10.1002/cjce.22241.

Buekers, J., Amery, F., Maes, A., Smolders, E., 2008. Long-term reactions of ni, zn and cd with iron oxyhydroxides depend on crystallinity and structure and on metal concentrations. Eur. J. Soil Sci. 59, 706–715. https://doi.org/10.1111/j.1365-2389.2008.01028.x.

Buerge-Weirich, D., Hari, R., Xue, H., Behra, P., Sigg, L., 2002. Adsorption of cu, cd, and ni on goethite in the presence of natural groundwater ligands. Environ. Sci. Technol. 36, 328–336. https://doi.org/10.1021/es010892i.

Cabral, A.R., Lehmann, B., Kwitko, R., Galbiatti, H.F., Pereira, M.C., 2002. Palladseite and its oxidation: evidence from Au-Pd vein-type mineralization (jacutinga), Cauê iron-ore mine, Quadrilátero Ferrífero, Minas Gerais, Brazil. Mineral. Mag. 66, 327–336. https://doi.org/10.1180/0026461026620033.

Camêlo, D.de L., Ker, J.C., Fontes, M.P.F., Corrêa, M.M., da Costa, A.C.S., Melo, V.F., 2017. Pedogenic iron oxides in iron-rich oxisols developed from mafic rocks. Rev. Bras. Ciênc. Solo 41, 1–16. https://doi.org/10.1590/18069657rbcs20160379.

Camêlo, D.de L., Ker, J.C., Fontes, M.P.F., da Costa, A.C.S., Corrêa, M.M., Leopold, M., 2018. Mineralogy, magnetic susceptibility and geochemistry of fe-rich oxisols developed from several parent materials. Sci. Agric. 75, 410–419. https://doi.org/10.1590/1678-992x-2017-0087.

Carmo, Flávio Fonseca do, Kamino, L.H.Y., Junior, R.T., Campos, I.C.de, Carmo, Felipe Fonseca do, Silvino, G., Castro, K.J.da S.X.de, Mauro, M.L., Rodrigues, N.U.A., Miranda, M.P.de S., Pinto, C.E.F., 2017. Fundão tailings dam failures: the environment tragedy of the largest technological disaster of Brazilian mining in global context. Perspect. Ecol. Conserv. 15, 145–151. https://doi.org/10.1016/j.pecon.2017.06.002.

Chen, C., Meile, C., Wilmoth, J., Barcellos, D., Thompson, A., 2018. Influence of pO 2 on iron redox cycling and anaerobic organic carbon mineralization in a humid tropical Forest soil. Environ. Sci. Technol. 52, 7709–7719. https://doi.org/10.1021/acs.est.8b01368.

Chukanov, N.V., 2014. Infrared spectra of mineral species. Springer Geochemistry/Mineralogy, Chernogolovka, Russia https://doi.org/10.1007/978-94-007-7128-4_2.

Cornell, R.M., Schwertmann, U., 2003. The Iron Oxides: Structure, Reactions, Occurences and Uses. WILEY-VCH https://doi.org/10.1002/3527602097.ch1.

Cuadros, J., Andrade, G., Ferreira, T.O., de Moya Partiti, C.S., Cohen, R., Vidal-Torrado, P., 2017. The mangrove reactor: fast clay transformation and potassium sink. Appl. Clay Sci. 140, 50–58. https://doi.org/10.1016/j.clay.2017.01.022.

Cui, H., Zhang, X., Wu, Q., Zhang, S., Xu, L., Zhou, Jing, Zheng, X., Zhou, Jun, 2020. Hematite enhances the immobilization of copper, cadmium and phosphorus in soil amended with hydroxyapatite under flooded conditions. Sci. Total Environ. 708, 134590. https://doi.org/10.1016/j.scitotenv.2019.134590.

Cummings, D.E., March, A.W., Bostick, B., Spring, S., Caccavo, F., Fendorf, S., Rosenzweig, R.F., Rosenzweig, R.Frank, 2000. Evidence for microbial Fe(III) reduction in anoxic, mining-impacted Lake sediments (Lake coeur d'Alene, Idaho). Appl. Environ. Microbiol. 66, 154–162.

Das, S., Hendry, M.J., 2014. Characterization of hematite nanoparticles synthesized via two different pathways. J. Nanopart. Res. 16, 2535. https://doi.org/10.1007/s11051-014-2535-7.

Du Laing, G., Rinklebe, J., Vandecasteele, B., Meers, E., Tack, F.M.G., 2009. Trace metal behaviour in estuarine and riverine floodplain soils and sediments: a review. Sci. Total Environ. 407, 3972–3985. https://doi.org/10.1016/j.scitotenv.2008.07.025.

Escobar, H., 2015. Mud tsunami wreaks ecological havoc in Brazil. Science (80-.) 350, 1138–1139. https://doi.org/10.1126/science.350.6265.1138.

Faivre, D., Frankel, R.B., 2016. Iron Oxides: From Nature to Applications. 1st ed. Wiley-VCH, Weinheim, Germany.

Ferreira, T.O., Otero, X.L., Vidal-Torrado, P., Macías, F., 2007a. Redox processes in mangrove soils under Rhizophora mangle in relation to different environmental conditions. Soil Sci. Soc. Am. J. 71, 484–491. https://doi.org/10.2136/sssaj2006.0078.

Ferreira, T.O., Otero, X.L., Vidal-Torrado, P., Macías, F., 2007b. Effects of bioturbation by root and crab activity on iron and sulfur biogeochemistry in mangrove substrate. Geoderma 142, 36–46. https://doi.org/10.1016/j.geoderma.2007.07.010.

Fink, J.R., Inda, A.V., Tiecher, T., Barrón, V., 2016. Iron oxides and organic matter on soil phosphorus availability. Cienc. Agrotecnol. 40, 369–379. https://doi.org/10.1590/1413-70542016404023016.

Fondo, E.N., Martens, E.E., 1998. Effects of mangrove deforestation on macrofaunal densities, Gazi Bay, Kenya. Mangroves Salt Marshes 2, 75–83. https://doi.org/10.1023/A:1009982900931.

Fontes, M.P.F., Weed, S.B., 1991. Iron oxides in selected Brazilian Oxisols: I. Mineralogy. Soil Sci. Soc. Am. J. 55, 1143–1149. https://doi.org/10.2136/sssaj1991.03615995005500040040x.

Fortin, D., Leppard, G.G., Tessier, A., 1993. Characteristics of lacustrine diagenetic iron oxyhydroxides. Geochim. Cosmochim. Acta 57, 4391–4404. https://doi.org/10.1016/0016-7037(93)90490-N.

Gabriel, F.A., Silva, A.G., Queiroz, H.M., Ferreira, T.O., Hauser-Davis, R.A., Bernardino, A.F., 2020. Ecological risks of metal and metalloid contamination in the Rio Doce estuary. Integr. Environ. Assess. Manag. 16, 655–660. https://doi.org/10.1002/ieam.4250.

Gama, F.F., Paradella, W.R., Mura, J.C., de Oliveira, C.G., 2019. Advanced DINSAR analysis on dam stability monitoring: a case study in the germano mining complex (Mariana, Brazil) with SBAS and PSI techniques. Remote Sens. Appl. Soc. Environ. 16. https://doi.org/10.1016/j.rsase.2019.100267.

Gao, X., Schulze, D.G., 2010. Precipitation and transformation of secondary fe oxyhydroxides in a histosol impacted by runoff from a lead smelter. Clay Clay Miner. 58, 377–387. https://doi.org/10.1346/CCMN.2010.0580308.

Gao, L., Li, R., Liang, Z., Wu, Q., Yang, Z., Li, M., Chen, J., Hou, L., 2021. Mobilization mechanisms and toxicity risk of sediment trace metals (Cu, Zn, Ni, and Pb) based on diffusive gradients in thin films: a case study in the Xizhi River basin, South China. J. Hazard. Mater. 410, 124590. https://doi.org/10.1016/j.jhazmat.2020.124590.

Glombitza, F., Reichel, S., 2014. Metal-containing residues from industry and in the environment: geobiotechnological Urban Mining. Adv. Biochem. Eng. Biotechnol. 141, 49–107. https://doi.org/10.1007/10_2013_254.

Gomes, L.E.de O., Correa, L.B., Sá, F., Neto, R.R., Bernardino, A.F., 2017. The impacts of the Samarco mine tailing spill on the Rio Doce estuary, Eastern Brazil. Mar. Pollut. Bull. 120, 28–36. https://doi.org/10.1016/j.marpolbul.2017.04.056.

Grossl, P.R., Sparks, D.L., Ainsworth, C.C., 1994. Rapid kinetics of Cu(II) adsorption/desorption on goethite. Environ. Sci. Technol. 28, 1422–1429. https://doi.org/10.1021/es00057a008.

Harford, A.J., Mooney, T.J., Trenfield, M.A., van Dam, R.A., 2015. Manganese toxicity to tropical freshwater species in low hardness water. Environ. Toxicol. Chem. 34, 2856–2863. https://doi.org/10.1002/etc.3135.

Hartley, W., Edwards, R., Lepp, N.W., 2004. Arsenic and heavy metal mobility in iron oxide-amended contaminated soils as evaluated by short- and long-term leaching tests. Environ. Pollut. 131, 495–504. https://doi.org/10.1016/j.envpol.2004.02.017.

Herbert, R.B., 1996. Metal retention by iron oxide precipitation from acidic ground water in Dalarna, Sweden. Appl. Geochem. 11, 229–235. https://doi.org/10.1016/0883-2927(95)00070-4.

Hochella, M.F., Kasama, T., Putnis, A., Putnis, C.V., Moore, J.N., 2005. Environmentally important, poorly crystalline Fe/Mn hydrous oxides: ferrihydrite and a possibly new vernadite-like mineral from the Clark Fork River superfund complex. Am. Mineral. 90, 718–724. https://doi.org/10.2138/am.2005.1591.

Howard, J., Hoyt, S., Isensee, K., Telszewski, M., Pidgeon, E., Telszewski, M., 2014. Coastal Blue Carbon: Methods for Assessing Carbon Stocks and Emissions Factors in Mangroves, Tidal Salt Marshes, and Seagrasses. Conservation International. Conservation International, Intergovernmental Oceanographic Commission of UNESCO, International Union for Conservation of Nature, Arlington, VA, USA, Arlington, VA, USA.

Huerta-Diaz, M.A., Morse, J.W., 1990. A quantitative method for determination of trace metal concentrations in sedimentary pyrite. Mar. Chem. 29, 119–144. https://doi.org/10.1016/0304-4203(90)90009-2.

Jackson, M.L., 2005. Soil Chemical Analysis: Advanced Course. 2nd ed. UW-Madison Libraries Parallel Press, Madison, Wisconsin.

Johnston, S.G., Keene, A.F., Bush, R.T., Burton, E.D., Sullivan, L.A., Isaacson, L., McElnea, A.E., Ahern, C.R., Smith, C.D., Powell, B., 2011. Iron geochemical zonation in a tidally inundated acid sulfate soil wetland. Chem. Geol. 280, 257–270. https://doi.org/10.1016/j.chemgeo.2010.11.014.

Jolivet, J.P., Chanéac, C., Tronc, E., 2004. Iron oxide chemistry. From molecular clusters to extended solid networks. Chem. Commun. 4, 477–483. https://doi.org/10.1039/b304532n.

Klug, H.P., Alexander, L.E., 1974. X-Ray Diffraction Procedures: For Polycrystalline and Amorphous Materials. 2nd ed. Wiley, New York.

Komárek, M., Vaněk, A., Ettler, V., 2013. Chemical stabilization of metals and arsenic in contaminated soils using oxides - a review. Environ. Pollut. 172, 9–22. https://doi.org/10.1016/j.envpol.2012.07.045.

Kosolapov, B.D.B., Kuschk, P., Vainshtein, M.B., Vatsourina, A.V., Wieûner, A., Kästner, M., Müller, R.A., 2004. Review Microbial Processes of Heavy Metal Removal from Carbon-Deficient Effluents in Constructed Wetlands, pp. 403–411 https://doi.org/10.1002/elsc.200420048.

Kraal, P., Burton, E.D., Rose, A.L., Kocar, B.D., Lockhart, R.S., Grice, K., Bush, R.T., Tan, E., Webb, S.M., 2015. Sedimentary iron–phosphorus cycling under contrasting redox conditions in a eutrophic estuary. Chem. Geol. 392, 19–31. https://doi.org/10.1016/j.chemgeo.2014.11.006.

Kukkadapu, R.K., Zachara, J.M., Smith, S.C., Fredrickson, J.K., Liu, C., 2001. Dissimilatory bacterial reduction of Al-substituted goethite in subsurface sediments. Geochim. Cosmochim. Acta 65, 2913–2924. https://doi.org/10.1016/S0016-7037(01)00656-1.

LaForce, M.J., Hansel, C.M., Fendorf, S., 2000. Constructing simple wetland sampling devices. Soil Sci. Soc. Am. J. 64, 809–811. https://doi.org/10.2136/sssaj2000.642809x.

Larsen, O., Postma, D., 2001. Kinetics of reductive bulk dissolution of lepidocrocite, ferrihydrite, and goethite. Geochim. Cosmochim. Acta 65, 1367–1379. https://doi.org/10.1016/S0016-7037(00)00623-2.

Liao, S., Wang, X., Yin, H., Post, J.E., Yan, Y., Tan, W., Huang, Q., Liu, F., Feng, X., 2020. Effects of Al substitution on local structure and morphology of lepidocrocite and its phosphate adsorption kinetics. Geochim. Cosmochim. Acta 276, 109–121. https://doi.org/10.1016/j.gca.2020.02.027.

Lindsay, W.L., 1991. Iron oxide solubilization by organic matter and its effect on iron availability. Plant Soil 130, 27–34. https://doi.org/10.1007/BF00011852.

Lovley, D.R., 1991. Dissimilatory Fe(III) and Mn(IV) reduction. Microbiol. Rev. 55, 259–287.

Lovley, D.R., Holmes, D.E., Nevin, K.P., 2004. Dissimilatory Fe(III) and Mn(IV) reduction. Adv. Microb. Physiol., 219–286 https://doi.org/10.1016/S0065-2911(04)49005-5.

Lu, L., 2015. Iron Ore: Mineralogy, Processing and Environmental Sustainability. 1st ed. Woodhead Publishing Series in Metals and Surface Engineering: Number 66. Elsevier, Sawston.

Machado, W., Borrelli, N.L., Ferreira, T.O., Marques, A.G.B., Osterrieth, M., Guizan, C., 2014. Trace metal pyritization variability in response to mangrove soil aerobic and anaerobic oxidation processes. Mar. Pollut. Bull. 79, 365–370. https://doi.org/10.1016/j.marpolbul.2013.11.016.

Manceau, A., Nagy, K.L., Spadini, L., Ragnarsdottir, K.V., 2000. Influence of anionic layer structure of fe-oxyhydroxides on the structure of cd surface complexes. J. Colloid Interface Sci. 228, 306–316. https://doi.org/10.1006/jcis.2000.6922.

Martínez, C.E., 1998. Coprecipitates of cd, cu, pb and zn in iron oxides: solid phase transformation and metal solubility after aging and thermal treatment. Clay Clay Miner. 46, 537–545. https://doi.org/10.1346/CCMN.1998.0460507.

Masue-Slowey, Y., Loeppert, R.H., Fendorf, S., 2011. Alteration of ferrihydrite reductive dissolution and transformation by adsorbed as and structural Al: implications for as retention. Geochim. Cosmochim. Acta 75, 870–886. https://doi.org/10.1016/j.gca.2010.11.016.

de Mello, C.R., Viola, M.R., Curi, N., da Silva, A.M., 2012. Distribuição espacial da precipitação e da erosividade da chuva mensal e anual no estado do Espírito Santo. Rev. Bras. Ciênc. Solo 36, 1878–1891. https://doi.org/10.1590/S0100-06832012000600022.

Melo, V.F., Fontes, M.P.F., Novais, R.F., Singh, B., Schaefer, C.E.G.R., 2001. Características dos óxidos de ferro e de alumínio de diferentes classes de solos. Rev. Bras. Ciênc. Solo 25, 19–32. https://doi.org/10.1590/s0100-06832001000100003.

Nielsen, O.I., Kristensen, E., Macintosh, D.J., 2003. Impact of fiddler crabs (Uca spp.) on rates and pathways of benthic mineralization in deposited mangrove shrimp pond waste. J. Exp. Mar. Biol. Ecol. https://doi.org/10.1016/S0022-0981(03)00041-8.

Nóbrega, G.N., Otero, X.L., Macías, F., Ferreira, T.O., 2014. Phosphorus geochemistry in a brazilian semiarid mangrove soil affected by shrimp farm effluents. Environ. Monit. Assess. 186, 5749–5762. https://doi.org/10.1007/s10661-014-3817-3.

Nóbrega, G.N., Ferreira, T.O., Artur, A.G., de Mendonça, E.S., de O. Leão, R.A., Teixeira, A.S., Otero, X.L., 2015. Evaluation of methods for quantifying organic carbon in mangrove soils from semi-arid region. J. Soils Sediments 15, 282–291. https://doi.org/10.1007/s11368-014-1019-9.

Otero, X.L., Ferreira, T.O., Huerta-Díaz, M.A., Partiti, C.S.M., Souza, V., Vidal-Torrado, P., Macías, F., 2009. Geochemistry of iron and manganese in soils and sediments of a mangrove system, island of pai matos (Cananeia — SP, Brazil). Geoderma 148, 318–335. https://doi.org/10.1016/j.geoderma.2008.10.016.

Otero, X.L., Araújo, J.M.C., Barcellos, D., Queiroz, H.M., Romero, D.J., Nóbrega, G.N., Neto, M.S., Ferreira, T.O., 2020. Crab bioturbation and seasonality control nitrous oxide emissions in semiarid mangrove forests (Ceará, Brazil). Appl. Sci. 10. https://doi.org/10.3390/app10072215.

Palau, J., Benaiges-Fernandez, R., Offeddu, F., Urmeneta, J., Soler, J.M., Cama, J., Dold, B., 2021. Release of trace elements during bioreductive dissolution of magnetite from metal mine tailings: potential impact on marine environments. Sci. Total Environ. 788, 147579. https://doi.org/10.1016/j.scitotenv.2021.147579.

Pan, W., Kan, J., Inamdar, S., Chen, C., Sparks, D., 2016. Dissimilatory microbial iron reduction release DOC (dissolved organic carbon) from carbon-ferrihydrite association. Soil Biol. Biochem. 103, 232–240. https://doi.org/10.1016/j.soilbio.2016.08.026.

Pansu, M., Gautheyrou, J., 2006. Handbook of soil analysis: mineralogical, organic and inorganic methods. Handbook of Soil Analysis: Mineralogical, Organic and Inorganic Methods https://doi.org/10.1007/978-3-540-31211-6.

Pereira, A.A., Van Hattum, B., Brouwer, A., Van Bodegom, P.M., Rezende, C.E., Salomons, W., 2008. Effects of iron-ore mining and processing on metal bioavailability in a tropical coastal lagoon. J. Soils Sediments 8, 239–252. https://doi.org/10.1007/s11368-008-0017-1.

Queiroz, H.M., Nóbrega, G.N., Ferreira, T.O., Almeida, L.S., Romero, T.B., Santaella, S.T., Bernardino, A.F., Otero, X.L., 2018a. The samarco mine tailing disaster: a possible time-bomb for heavy metals contamination? Sci. Total Environ. 637–638, 498–506. https://doi.org/10.1016/j.scitotenv.2018.04.370.

Queiroz, H.M., Nóbrega, G.N., Otero, X.L., Ferreira, T.O., 2018b. Are acid volatile sulfides (AVS) important trace metals sinks in semi-arid mangroves? Mar. Pollut. Bull. 126, 318–322. https://doi.org/10.1016/j.marpolbul.2017.11.020.

Queiroz, H.M., Ferreira, T.O., Barcellos, D., Nóbrega, G.N., Antelo, J., Otero, X.L., Bernardino, A.F., 2021a. From sinks to sources: the role of fe oxyhydroxide transformations on phosphorus dynamics in estuarine soils. J. Environ. Manag. 278, 111575. https://doi.org/10.1016/j.jenvman.2020.111575.

Queiroz, H.M., Ying, S.C., Abernathy, M., Barcellos, D., Gabriel, F.A., Otero, X.L., Nóbrega, G.N., Bernardino, A.F., Ferreira, T.O., 2021b. Manganese: the overlooked contaminant in the world largest mine tailings dam collapse. Environ. Int. 146, 106284. https://doi.org/10.1016/j.envint.2020.106284.

Randall, S.R., Sherman, D.M., Ragnarsdottir, K.V., Collins, C.R., 1999. The mechanism of cadmium surface complexation on iron oxyhydroxide minerals. Geochim. Cosmochim. Acta 63, 2971–2987. https://doi.org/10.1016/S0016-7037(99)00263-X.

Reddy, K.R., DeLaune, R.D., 2008. Biogeochemistry of Wetlands: Science and Applications. 1st ed. CRC Press.

Rehman, F., Pervez, A., Khattak, B.N., Ahmad, R., 2017. Constructed wetlands: perspectives of the oxygen released in the rhizosphere of macrophytes. Clean: Soil, Air, Water 45. https://doi.org/10.1002/clen.201600054.

Roden, E.E., Zachara, J.M., 1996. Microbial reduction of crystalline Iron(III) oxides: influence of oxide surface area and potential for cell growth. Environ. Sci. Technol. 30, 1618–1628. https://doi.org/10.1021/es9506216.

Rose, A.W., Bianchi-Mosquera, G.C., 1993. Adsorption of cu, pb, zn co, ni, and ag on goethite and hematite; a control on metal mobilization from red beds into stratiform copper deposits. Econ. Geol. 88, 1226–1236. https://doi.org/10.2113/gsecongeo.88.5.1226.

Ruan, H.D., Gilkes, R.J., 1995. Dehydroxylation of aluminous goethite: unit cell dimensions, crystal size and surface area. Clay Clay Miner. 43, 196–211. https://doi.org/10.1346/CCMN.1995.0430207.

Ruan, H.D., Frost, R.L., Kloprogge, J.T., Duong, L., 2002. Infrared spectroscopy of goethite dehydroxylation: III. FT-IR microscopy of in situ study of the thermal transformation of goethite to hematite. Spectrochim. Acta A Mol. Biomol. Spectrosc. 58, 967–981. https://doi.org/10.1016/S1386-1425(01)00574-1.

Rutten, A., de Lange, G.J., 2003. Sequential extraction of iron, manganese and related elements in S1 sapropel sediments, eastern Mediterranean. Palaeogeogr. Palaeoclimatol. Palaeoecol. 190, 79–101. https://doi.org/10.1016/S0031-0182(02)00600-4.

Sarker, S., Masud-Ul-Alam, M., Hossain, M.S., Rahman Chowdhury, S., Sharifuzzaman, S., 2020. A review of bioturbation and sediment organic geochemistry in mangroves. Geol. J. https://doi.org/10.1002/gj.3808.

Schulze, D.G., 1981. Identification of soil iron oxide minerals by differential X-ray diffraction. Soil Sci. Soc. Am. J. 45, 437–440. https://doi.org/10.2136/sssaj1981.03615995004500020040x.

Schwertmann, U., 1988. Occurrence and formation of iron oxides in various pedoenvironments. Iron in Soils and Clay Minerals. Springer Netherlands, Dordrecht, pp. 267–308 https://doi.org/10.1007/978-94-009-4007-9_11.

Schwertmann, U., 1991. Solubility and dissolution of iron oxides. Plant Soil https://doi.org/10.1007/BF00011851.

Schwertmann, U., Fitzpatrick, R.W., 1992. Iron minerals in surface environments. Catena Suppl. 21, 7–30.

Schwertmann, U., Taylor, R.M., 1989. Iron oxides. Minerals in Soil Environments. Soil Science Society of America, Madison, Wisconsin, pp. 379–438 https://doi.org/10.2136/sssabookser1.2ed.c8.

Schwertmann, U., Schulze, D.G., Murad, E., 1982. Identification of ferrihydrite in soils by dissolution kinetics, differential X-ray diffraction, and Mössbauer spectroscopy. Soil Sci. Soc. Am. J. 46, 869–875. https://doi.org/10.2136/sssaj1982.03615995004600040040x.

Schwertmann, U., Friedl, J., Stanjek, H., Schulze, D.G., 2000. The effect of Al on fe oxides. XIX. Formation of Al-substituted hematite from ferrihydrite at 25°C and pH 4 to 7. Clay Clay Miner. 48, 159–172. https://doi.org/10.1346/CCMN.2000.0480202.

Seybold, C.A., Mersie, W., Huang, J., McNamee, C., 2002. Soil redox, pH, temperature, and water-table patterns of a freshwater tidal wetland. Wetlands 22, 149–158. https://doi.org/10.1672/0277-5212(2002)022[0149:SRPTAW]2.0.CO;2.

Sherameti, I., Varma, A., 2015. Heavy Metal Contamination of Soils, Soil Biology. Springer International Publishing, Cham https://doi.org/10.1007/978-3-319-14526-6.

Silva, R.C.F., Ardisson, J.D., Cotta, A.A.C., Araujo, M.H., Teixeira, A.P.de C., 2020. Use of iron mining tailings from dams for carbon nanotubes synthesis in fluidized bed for 17α-ethinylestradiol removal. Environ. Pollut., 260 https://doi.org/10.1016/j.envpol.2020.114099.

Silva, A.C., Cavalcante, L.C.D., Fabris, J.D., Júnior, R.F., Barral, U.M., Viana, A.J.S., Ardisson, J.D., Fernandez-Outon, L.E., Lara, L.R.S., Stumpf, H.O., Barbosa, J.B.S., Silva, L.C.da, Farnezi, M.M.de M., 2016. Características químicas, mineralógicas e físicas do material acumulado em terraços fluviais, originado do fluxo de lama proveniente do rompimento de barragem de rejeitos de mineração de ferro em Bento Rodrigues, Minas Gerais, Brasil. Rev. Espinhaço 5 (2), 44–53. https://doi.org/10.5281/zenodo.3957942.

Singh, B., Gilkes, R.J., 1992. Properties and distribution of iron oxides and their association with minor elements in the soils of South-Western Australia. J. Soil Sci. 43, 77–98. https://doi.org/10.1111/j.1365-2389.1992.tb00121.x.

Siregar, A., Kleber, M., Mikutta, R., Jahn, R., 2005. Sodium hypochlorite oxidation reduces soil organic matter concentrations without affecting inorganic soil constituents. Eur. J. Soil Sci. 56, 481–490. https://doi.org/10.1111/j.1365-2389.2004.00680.x.

Slomp, C.P., Van Der Gaast, S.J., Van Raaphorst, W., 1996. Phosphorus binding by poorly crystalline iron oxides in North Sea sediments. Mar. Chem. 52, 55–73. https://doi.org/10.1016/0304-4203(95)00078-X.

Strauss, R., Brummer, G.W., Barrow, N.J., 1997. Effects of crystallinity of goethite: II. Rates of sorption and desorption of phosphate. Eur. J. Soil Sci. 48, 101–114. https://doi.org/10.1111/j.1365-2389.1997.tb00189.x.

Stumm, W., Morgan, J.J., 1996. Aquatic Chemistry: Chemical Equilibria and Rates in Natural Waters. 3rd ed. John Wiley & Sons, Inc, Danvers.

Tack, F.M.G., Van Ranst, E., Lievens, C., Vandenberghe, R.E., 2006. Soil solution cd, cu and zn concentrations as affected by short-time drying or wetting: the role of hydrous oxides of fe and mn. Geoderma 137, 83–89. https://doi.org/10.1016/j.geoderma.2006.07.003.

Tessier, A., Campbell, P.G.C., Bisson, M., 1979. Sequential extraction procedure for the speciation of particulate trace metals. Anal. Chem. 51, 844–851. https://doi.org/10.1021/ac50043a017.

Thompson, A., Rancourt, D.G., Chadwick, O.A., Chorover, J., 2011. Iron solid-phase differentiation along a redox gradient in basaltic soils. Geochim. Cosmochim. Acta 75, 119–133. https://doi.org/10.1016/j.gca.2010.10.005.

Trivedi, P., Axe, L., 2001. Ni and zn sorption to amorphous versus crystalline iron oxides: macroscopic studies. J. Colloid Interface Sci. 244, 221–229. https://doi.org/10.1006/jcis.2001.7970.

Velde, B., Peck, T., 2002. Clay mineral changes in the morrow experimental plots, University of Illinois. Clays Clay Miner. 50, 364–370. https://doi.org/10.1346/000986002760833738.

Violante, A., Barberis, E., Pigna, M., Boero, V., 2003. Factors affecting the formation, nature, and properties of iron precipitation products at the soil-root interface. J. Plant Nutr. 26, 1889–1908. https://doi.org/10.1081/PLN-120024252.

Wang, X., Li, W., Harrington, R., Liu, F., Parise, J.B., Feng, X., Sparks, D.L., 2013. Effect of ferrihydrite crystallite size on phosphate adsorption reactivity. Environ. Sci. Technol. 47, 10322–10331. https://doi.org/10.1021/es401301z.

Wang, X., Zhu, M., Lan, S., Ginder-Vogel, M., Liu, F., Feng, X., 2015. Formation and secondary mineralization of ferrihydrite in the presence of silicate and Mn(II). Chem. Geol. 415, 37–46. https://doi.org/10.1016/j.chemgeo.2015.09.009.

Wang, P., Wang, J., Zhang, H., Dong, Y., Zhang, Y., 2019. The role of iron oxides in the preservation of soil organic matter under long-term fertilization. J. Soils Sediments 19, 588–598. https://doi.org/10.1007/s11368-018-2085-1.

Wilson, G.V., Rhoton, F.E., Selim, H.M., 2004. Modeling the impact of ferrihydrite on adsorption-desorption of soil phosphorus. Soil Sci. 169, 271–281. https://doi.org/10.1097/01.ss.0000126841.03965.3a.

Winkler, P., Kaiser, K., Thompson, A., Kalbitz, K., Fiedler, S., Jahn, R., 2018. Contrasting evolution of iron phase composition in soils exposed to redox fluctuations. Geochim. Cosmochim. Acta 235, 89–102. https://doi.org/10.1016/j.gca.2018.05.019.

Zachara, J.M., Fredrickson, J.K., Smith, S.C., Gassman, P.L., 2001. Solubilization of Fe(III) oxide-bound trace metals by a dissimilatory Fe(III) reducing bacterium. Geochim. Cosmochim. Acta 65, 75–93. https://doi.org/10.1016/S0016-7037(00)00500-7.

Zhang, S., Xue, X., Liu, X., Duan, P., Yang, H., Jiang, T., Wang, D., Liu, R., 2006. Current situation and comprehensive utilization of iron ore tailing resources. J. Min. Sci. 42, 403–408. https://doi.org/10.1007/s10913-006-0069-9.

Zheng, X., Xu, X., Xu, K., 2011. Study on the risk assessment of the tailings dam break. Procedia Eng. 26, 2261–2269. https://doi.org/10.1016/j.proeng.2011.11.2433.